Delta University Scientific Journal
Journal home page: https://dusj.journals.ekb.eg

Development of a Mixed Numerical Method for Piled-Raft Analysis Using International Codes

Ibrahim El Arabi [1]*, ***Mohamed El Gendy*** [2], ***Mohamed A. Kamal*** [3]

[1] *Assoc. Prof., Civil Engineering Dept., Delta Univ. for Science and Technology, Mansoura, Egypt*
[2] *Prof., Civil Engineering Dept., Faculty of Engineering, Port Said University, Port Said, Egypt*
[3] *PhD., Civil Engineer, General Authority for Port-Said Ports, Port Said, Egypt*

* **Correspondence:** *Assoc. Prof., Civil Engineering Dept. , Delta Univ. for Science and Technology, Mansoura, Egypt, Ibrahim.alarabi@deltauniv.edu.eg.com, https://orcid.org/0000-0002-0105-9341 .*

ABSTRACT

In previous research (El-Gendy et al., 2013), the authors presented a modified hyperbolic load-settlement model for bored piles, which depends on the ultimate loads predicted by relevant international codes (ECP202, 2005; DIN4014, 1990; AASHTO, 2005; French Code, 1993). This research presents a mixed numerical method to analyze vertically-loaded piled-rafts comprising large-diameter bored piles. To determine the stiffness matrix of piled-raft, the pile-self settlement is simulated by using any of the four indicated codes or by the modified load-settlement model. Interactions among the different components of the piled-raft system are found using the elasticity theory. Analysis is performed iteratively until compatibility among raft, pile, and soil is ensured at all interfaces. The validity of the proposed method is established by comparing the predicted settlements and pile load ratios to field measurements for nine published case histories. The results showed that DIN4014 mostly gives the closest match to field measurements.

Keywords: Piled-raft; Bored-piles; Pile load-settlement model; Settlement; Pile load ratio.

1. Introduction

Many authors studied the nonlinear response of pile-soil system using theoretical relations between the load and settlement (Mandolini & Viggiani., 1997; Viggiani, 1998; Russo, 1998). Many others investigated the settlement behavior and load-carrying capacity of piled raft systems for various soil conditions using different types of numerical methods (Huang *et al.*, 2017; Nguyen *et al.*, 2021), among others. Besides, most international codes, such as Egyptian, German, American, and French codes (ECP202, 2005; DIN4014, 1990; AASHTO, 2005; French Code, 1993), present empirical load-settlement relationships for single piles. Based on the ultimate pile load predicted by the code, the authors (El-Gendy *et al.*, 2013) proposed a simplified hyperbolic load-settlement model for large-diameter bored-piles. Moreover, the second author with others presented a mixed method for the analysis of piled-raft systems based on both empirical and mathematical models (El-Gendy *et al.*, 2006). They modeled the pile itself settlement using the empirical load-settlement model given by German code (DIN4014, 1990), whereas the settlements due to pile-pile, pile-raft, and raft-soil interactions were determined using flexibility coefficients based on Mindlin's solution (Mindlin, 1936). The compatibility between the settlements of piles, raft, and soil should be fully ensured for all pile-raft-soil interfaces. The main objective of this research is to validate the indicated mixed piled raft analysis when using Egyptian, American, and French codes (ECP202, 2005; AASHTO, 2005; French Code, 1993), instead of using German code (DIN4014, 1990). The hyperbolic load-settlement model proposed previously by the authors (El-Gendy *et al.*, 2013) is also validated for the analysis of piled-raft using the indicated mixed method (El Gendy *et al.*, 2006). Nine piled-raft case histories, for which the building behavior has been monitored using instruments, are re-analyzed herein. Both the numerically predicted and measured settlements as well as the pile load-sharing ratios for every case history are compared for validation.
At first, the authors' proposed load-settlement model of large-diameter bored-piles is presented. Then, the basic formulation of piled-raft analysis is given. The main steps of the iterative method and the flow chart of the

analysis method are then illustrated. Numerical applications on nine case histories of piled-raft systems are presented and the comparisons between predictions and measured results are discussed.

2. Numerical modeling

2.1. Pile itself settlement.

In the present analysis of a piled-raft system, it is assumed that the settlement along the entire length of the pile is the same as the pile tip settlement. It is essential to adopt an appropriate model to simulate the nonlinear relationship between the pile load and the corresponding settlement. The empirical load-settlement relationship given by any of the four codes indicated above may be used. Alternatively, one may use the following load-settlement hyperbolic model (El-Gendy *et al.*, 2013):

$$Q = \frac{11\,Q_u}{\frac{S_u}{S} + C} \quad \textbf{(1)}$$

where:

Q_u Ultimate pile load predicted by the code, [kN],
S_u Ultimate settlement recommended by the code, [cm],
Q Pile load corresponding to any settlement S, [kN], and
C Coefficient equals 8.66 for ECP 202 and French codes and equals 11 for DIN4014 and AASHTO codes.

Figure 1 shows samples of the proposed hyperbolic; and empirical multi-linear load-settlement curves. The pile self-load and self-settlement are related to each other by:

$$Qp_i = Sp_i \tan k_i \quad \textbf{(2)}$$

where:

Qp_i Load on pile i, [kN],
Sp_i Self-settlement of pile i, [m], and
$\tan k_i$ Ratio between the pile load and pile settlement, [kN/m].

For a pile group consists of n-piles, Equation (2) is written in a matrix form as:

$$\{Qp\} = [Kp]\{Sp\} \quad \textbf{(3)}$$

where:

$\{Qp\}$ vector of pile loads,
$[Kp]$ $n \times n$ diagonal matrix represents the soil stiffness resulting from pile self-settlements, and
$\{Sp\}$ vector of self-settlements for piles.

In order to start the computations in any nonlinear analysis of a pile group or a piled-raft, an initial value should be assigned to the pile stiffness K_i. This value may be taken as the slope of the secant $K_i^{(o)}$ of the load-settlement curve at point 1 as shown in Figure 1, where $Sp=Srg$. Therefore, $K_i^{(o)} = Qt / Srg$. Equation (3) may be written in another form as:

$$\{Sp\} = [Cp]\{Qp\} \quad \textbf{(4)}$$

where [Cp] is an $n_p \times n_p$ diagonal matrix, which represents the soil flexibility due to pile self-settlements, and equals the inverse of the stiffness matrix [Kp].

2.2. Pile-pile interaction

The total pile resistance is the sum of the tip resistance acting at its base, and friction resistance distributed along its shaft. For a pile j, both resistance components may produce the following settlement components in another pile i:

a) Settlement along the pile shaft $Sbs_{i,j}$ [m] due to a tip force Qb_j [kN],
b) Settlement at the pile base $Sbb_{i,j}$ [m] due to a tip force Qb_j [kN],
c) Settlement along the pile shaft $Sss_{i,j}$ [m] due to a skin friction force Qs_j [kN], and
d) Settlement at the pile base $Ssb_{i,j}$ [m] due to a skin friction force Qs_j [kN].

All settlement components are computed by Mindlin's solution (Mindlin, 1936). Referring to Figure 2 which gives the settlement $S_{k,j}$ at a point k at a depth z from the ground surface; due to a vertical force Q_j acting at a point j. In this case

$$S_{k,j} = f_{k,j} Q_j \quad \textbf{(5)}$$

where $f_{k,j}$ is given by Mindlin's solution (Mindlin, 1936) as:

$$f_{k,j} = \frac{1}{16\,\pi\,G_s\,(1-\nu_s)}\left(\frac{3-4\,\nu_s}{R_1} + \frac{8\,(1-\nu_s)^2-(3-4\nu_s)}{R_2} + \frac{(z-c)^2}{R_1^3} + \frac{(3-4\,\nu_s)(z+c)^2-2cz}{R_2^3} + \frac{6\,c\,z\,(z+c)^2}{R_2^5}\right) \quad \textbf{(6)}$$

where:

$R_1 = \sqrt{r^2+(z-c)^2}$, $R_2 = \sqrt{r^2+(z+c)^2}$ and

c Depth of the point load Q_j from the ground surface, [m],
z Depth of the studied point k from the ground surface, [m],
r Radial distance between points k and j, [m],
z-c Vertical distance between points k and j, [m],
z+c Vertical distance between points k and w, [m],
$f_{k,j}$ Flexibility coefficient of point k due to a unit load at point j, [m/kN],
G_s Shear modulus of the soil, $G_s = 0.5\,E_s / (1+\nu_s)$, [kN/m^2],
E_s Elasticity modulus of the soil, [kN/m^2],
ν_s *Poisson's* ratio of the soil, [-].

Referring to Figure 3, the shaft settlement $Sbs_{i,j}$ along a pile i due to the force Qb_j acting at the tip of a pile j can be expressed as:

$$Sbs_{i,j} = \frac{1}{l_i}\int_{z_1}^{z_2} Sbs_{k,j}\,dz \quad \textbf{(7)}$$

where the total length l_i [m] of pile i is subdivided into m elements of constant length Δl [m]. It is better to carry out the integration in Equation (7) numerically to deal equally with homogeneous as well as with multi-layered soil. Equation (7) can be written as:

$$Sbs_{i,j} = F_{i,j}\,Qb_j \quad \textbf{(8)}$$

where $F_{i,j}$ [m/kN] is the shaft flexibility coefficient of a pile i due to a force Qb_j acting at the base of a pile j.

The tip settlement $Sbb_{i,j}$ at the base of a pile i due to a force Qb_j at the base of pile j can be expressed as:

$$Sbb_{i,j} = F_{b,j}\,Qb_j \quad \textbf{(9)}$$

where $F_{b,j}$ [m/kN] is the base flexibility coefficient of a pile i due to a tip force Qb_j acting at the base of pile j.

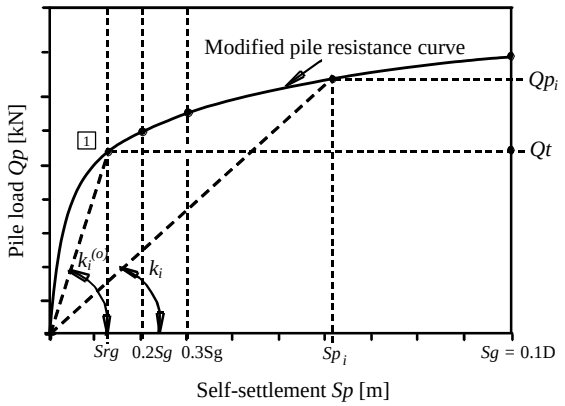

S_g = 0.1 D D = Pile shaft diameter

(a) Proposed load-settlement model

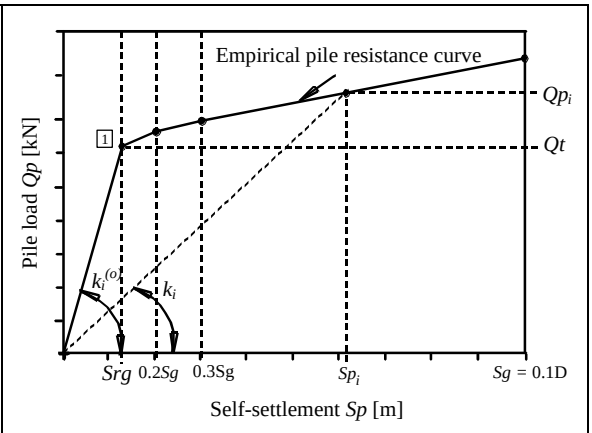

S_{rg} = 0.5 Q_{rg} + 0.5 ≤ 3 Q_{rg} Ultimate skin resistance force [MN]

(b) DIN 4014 load-settlement curve

Fig. (1): Relation between the self-settlement in the pile and its load for a single bored-pile

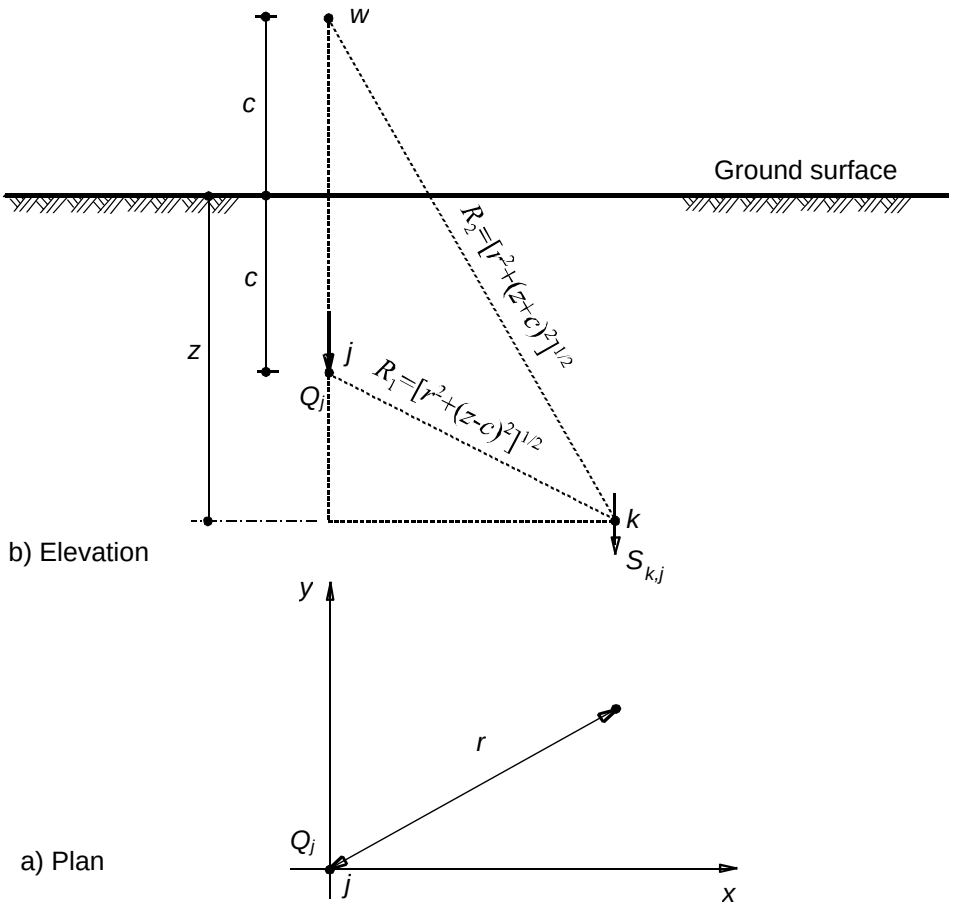

Fig. (2): Geometry of Mindlin's problem

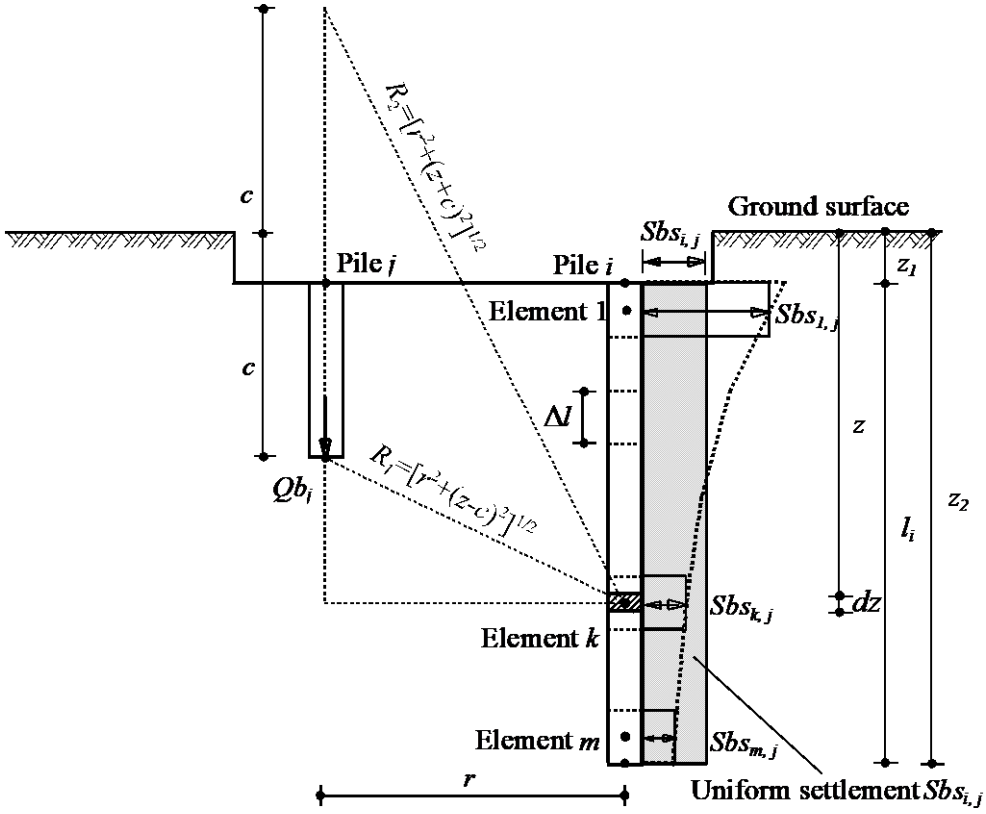

Fig. (3): Settlement $Sbs_{k,j}$ in an element k of pile i due to a tip force Qb_j at the base of pile j

Assuming that the settlement is uniform along the entire pile shaft, the base settlement can be taken the same as the settlement along the shaft. The settlement $Sb_{i,j}$ of a pile i due to the tip force Qb_j acting at the base of pile j, can be approximated as the average of the shaft and the base settlements computed separately from Equations (8) and (9). Therefore

$$Sb_{i,j} = Fb_{i,j}\, Qb_j \tag{10}$$

where $Fb_{i,j}$= 0.5 ($F_{i,j}$+$F_{b,j}$), is the flexibility coefficient of a pile i due to a tip force Qb_j acting at the base of pile j, [m/kN].

For a pile group consists of n piles, the pile-pile interaction settlement can be written in a matrix form as:

$$\{Sb\} = [Fb]\{Qb\} \tag{11}$$

where:

$\{Sb\}$ n vector of settlements in piles due to forces acting on the pile bases.

$\{Qb\}$ n vector of forces acting on the pile bases.

$[Fb]$ $n \times n$ matrix of pile flexibility coefficients due to unit tip forces on piles, $Fb_{i,i} = 0$.

Figure 4 shows a system consists of two piles, in which a shaft element k of a pile i is influenced by a skin friction τs_j [kN/m^2] acting on the shaft perimeter of a pile j; with a diameter d_j [m] and a length l_j [m]. The skin friction along the shaft perimeter of pile j is represented by a total skin friction force Qs_j [kN] = $\pi\ d_j\ l_j\ \tau s_j$. To avoid extensive computations when applying Mindlin's solution (Mindlin, 1936) to determine the flexibility coefficients due to shaft stress along the pile shaft, the shaft stress τs_j is replaced by an equivalent line load T [kN/m] = Qs_j / l_j acting on the axis of the pile. The settlement $Sss_{k,j}$ in a point k at a depth z from the surface due to a total skin force Qs_j on a pile j is expressed as:

$$Sss_{k,j} = I_{k,j}\, Qs_j \tag{12}$$

where $I_{k,j}$ [m/kN] is the flexibility coefficient of a point k due to the total skin friction force Qs_j on pile j. This flexibility coefficient is determined from Eq. (6) by integrating the coefficient of a point load [$dQs_j = T\ dc$] over the length of pile j. The flexibility coefficient $I_{k,j}$ of a point k due to a unit skin force on pile j can be obtained from:

$$I_{k,j} = \frac{1}{l_j}\int_{c_1}^{c_2} f_{k,j}\, dc \tag{13}$$

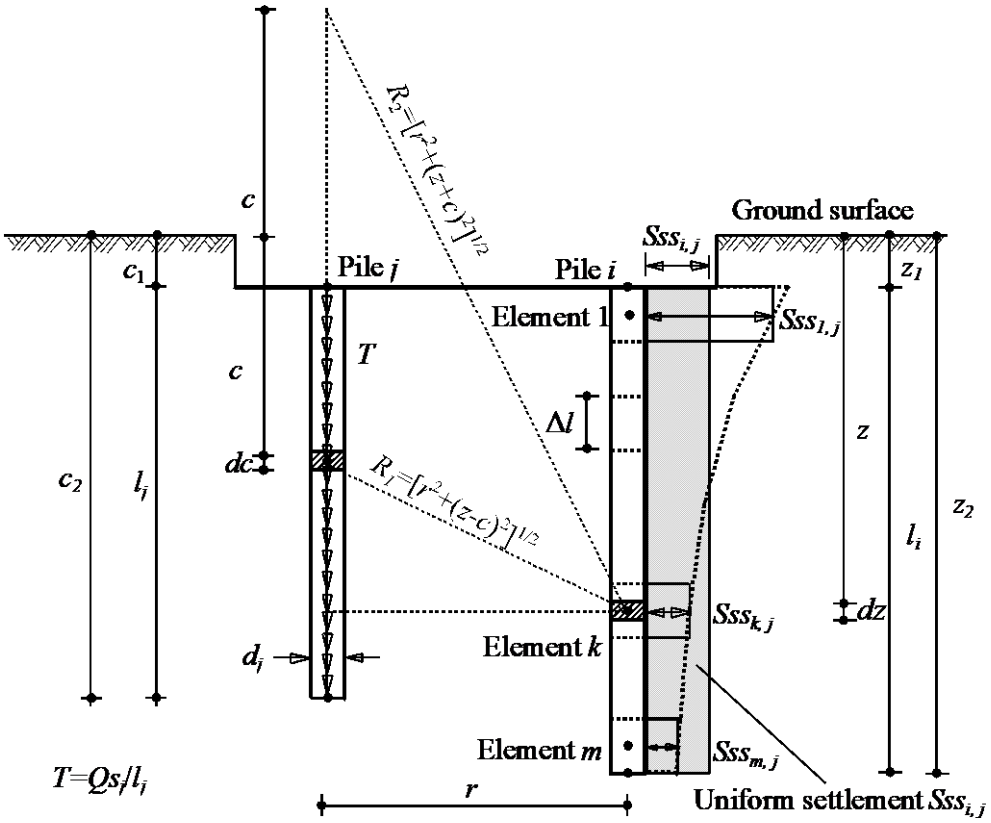

Fig. (4): Settlement $Sss_{k,j}$ in an element k of pile i due to a skin force $Qs_j = T_j\ l_j$ on pile j

This yields to:

$$I_{k,j} = \frac{1}{16\,\pi\, l_j\, G_s\,(1 - v_s)}\,(I_1 + I_2 + I_3 + I_4 + I_5) \tag{14}$$

where I_1 to I_5 are given by:

$$I_1 = (3 - 4\,v_s)\ln\left[\frac{\sqrt{r^2 + (z - c_2)^2} - (z - c_2)}{\sqrt{r^2 + (z - c_1)^2} - (z - c_1)}\right] \tag{15}$$

$$I_2 = \left[8\,(1 - v_s)^2 - (3 - 4\,v_s)\right]\ln\left[\frac{\sqrt{r^2 + (z + c_2)^2} + (z + c_2)}{\sqrt{r^2 + (z + c_1)^2} + (z + c_1)}\right] \tag{16}$$

$$I_3 = \ln\left[\frac{\sqrt{r^2 + (z - c_2)^2} - (z - c_2)}{\sqrt{r^2 + (z - c_1)^2} - (z - c_1)}\right] + \frac{z - c_2}{\sqrt{r^2 + (z - c_2)^2}} - \frac{z - c_1}{\sqrt{r^2 + (z - c_1)^2}} \tag{17}$$

$$\begin{aligned} I_4 = (3 - 4\,v_s)\Bigg(&\ln\left[\frac{\sqrt{r^2 + (z + c_2)^2} + (z + c_2)}{\sqrt{r^2 + (z + c_1)^2} + (z + c_1)}\right] - \frac{(z + c_2)}{\sqrt{r^2 + (z + c_2)^2}} \\ &+ \frac{(z + c_1)}{\sqrt{r^2 + (z + c_1)^2}}\Bigg) - 2\,z\left(\frac{1}{\sqrt{r^2 + (z + c_1)^2}} - \frac{1}{\sqrt{r^2 + (z + c_2)^2}}\right. \\ &\left. + \frac{z\,(z + c_1)}{r^2\sqrt{r^2 + (z + c_1)^2}} - \frac{z\,(z + c_2)}{r^2\sqrt{r^2 + (z + c_2)^2}}\right) \end{aligned} \tag{18}$$

$$I_5 = \frac{6\,z\left[r^4 - z\,(z + c_2)^3\right]}{3\,r^2\left[r^2 + (z + c_2)^2\right]^{3/2}} - \frac{6\,z\left[r^4 + z\,(z + c_1)^3\right]}{3\,r^2\left[r^2 + (z + c_2)^2\right]^{3/2}} - \frac{6\,z}{\sqrt{r^2 + (z + c_2)^2}} + \frac{6\,z}{\sqrt{r^2 + (z + c_1)^2}} \tag{19}$$

where:

c_1 Starting depth of the line load T from the surface, [m],
c2 End depth of the line load T from the surface, [m],
lj Length of the line load T, [m], and
r Radial distance between points k and j [m].

The uniform settlement $Sss_{i,j}$ along the shaft of a pile i due to a skin force Qs_j on pile j can be obtained by using the same approach used for determining the uniform settlement due to a tip force on the base. Similar to Equation (5), $Sss_{i,j}$ can be expressed as:

$$Sss_{i,j} = L_{i,j}\,Qs_j \tag{20}$$

where $L_{i,j}$ [m/kN] is the shaft flexibility coefficient of a pile i due to a skin force Qs_j on pile j. The shaft flexibility coefficient $L_{i,j}$ is given by:

$$L_{i,j} = \frac{\Delta l}{l_i}\left(I_{1,j} + I_{2,j} + I_{3,j} + I_{4,j} + \ldots + I_{m,j}\right) \tag{21}$$

The settlement $Ssb_{i,j}$ at the base of a pile i due to a skin force Qs_j on pile j is expressed by:

$$Ssb_{i,j} = L_{b,j}\, Qs_j \quad \textbf{(22)}$$

where $L_{b,j}$ [m/kN] is the base flexibility coefficient of a pile i due to a skin force Qs_j on pile j. The base flexibility coefficient is determined from Eq. (12) by taking $z = z_2$.
Similar to Equation (10), the settlement in the pile is obtained from:

$$Ss_{i,j} = Is_{i,j}\, Qs_j \quad \textbf{(23)}$$

where $Is_{i,j}$= 0.5 ($L_{i,j}$+$L_{b,j}$), is the flexibility coefficient of a pile i due to a skin force Qs_j acting on pile j, [m/kN].
Similar to Equation (11), the settlement Ss_i for a group consists of n piles is given in a matrix form by:

$$\{Ss\} = [Is]\{Qs\} \quad \textbf{(24)}$$

where:
$\{Ss\}$ n vector of settlements in the piles due to skin forces of the piles,
$[Is]$ $n \times n$ matrix of pile flexibility coefficients due to unit skin forces acting on the piles, $Is_{i,i} = 0$.
$\{Qs\}$ n vector of skin forces acting on the piles.

2.3. Pile-raft interaction

In the same manner, the settlement $Sr_{i,j}$ [m] in a pile i due to a contact force Qr_j [kN] acting at a node j located at the contact surface between the raft and soil is given by:

$$Sr_{i,j} = Jr_{i,j}\, Qr_j \quad \textbf{(25)}$$

where $Jr_{i,j}$ is the flexibility coefficient of a pile i due to a contact force Qr_j acting at node j on the raft, [m/kN].
For a group consists of n piles, settlements in piles due to contact forces acting on the raft are expressed as:

$$\{Sr\} = [Jr]\{Qr\} \quad \textbf{(26)}$$

where:
$\{Sr\}$ n_p vector of settlements in piles due to contact forces on the raft,
$[Jr]$ $n_p \times n_r$ matrix of pile flexibility coefficients due to unit contact forces, and
$\{Qr\}$ n_r vector of contact forces on the raft.
The total settlement in a pile i due to all forces in the piled-raft system is given by:

$$\{St\} = \{Sp\} + \{Sb\} + \{Ss\} + \{Sr\} \quad \textbf{(27)}$$

where:
$\{St\}$ n_p vector of total settlements in piles due to all forces in the piled-raft system. Substituting from Equations (4), (11), (24) and (26) into Equation (27), it can be found that:

$$\{St\} = [Cp]\{Qp\} + [Fb]\{Qb\} + [Is]\{Qs\} + [Jr]\{Qr\} \quad \textbf{(28)}$$

2.4. Raft-pile interaction

In the same manner, the settlement at any node i on the raft due to both pile base and shaft forces can be determined. The settlement $Wb_{i,j}$ [m] at a node i on the raft due to a tip force Qb_j acting at the base of pile j is given by:

$$Wb_{i,j} = Cb_{i,j}\, Qb_j \quad \textbf{(29)}$$

Where $Cb_{i,j}$ [m/kN] is the flexibility coefficient of node i due to a tip force Qb_j acting at the base of pile j.
Similarly, the settlement $Wb_{i,j}$ [m] in a node i on the raft due to a skin force Qs_j on pile j is given by:

$$Ws_{i,j} = Cs_{i,j}\, Qs_j \quad \textbf{(30)}$$

where $Cs_{i,j}$ [m/kN] is the flexibility coefficient of node i due to a skin force Qs_j on pile j. The flexibility coefficients $Cb_{i,j}$ and $Cs_{i,j}$ are obtained directly from Equations (6) and (14), respectively.
For a raft consists of n_r nodes, Equation (29) can be written in a matrix form as:

$$\{Wb\} = [Cb]\{Qb\} \quad \textbf{(31)}$$

where:
$\{Wb\}$ n_r vector of settlements at the nodes of the raft due to pile base forces, and
$[Cb]$ $n_r \times n_p$ matrix of raft flexibility coefficients due to unit tip forces on piles.

Similarly, for a raft consists of n_r nodes, Equation (30) is written as:

$$\{Ws\} = [Cs]\{Qs\} \quad \textbf{(32)}$$

where:
$\{Ws\}$ n_r vector of settlements at the nodes of the raft due to skin forces, and
$[Cs]$ $n_r \times n_p$ matrix of raft flexibility coefficients due to unit skin forces on piles.

2.5. Raft-soil interaction

Settlements at the raft nodes due to contact forces on the raft can also be determined from Mindlin's solution (Mindlin, 1936). The flexibility coefficients for a contact force on the raft are obtained from Equation (6). This is applicable for all nodes except for the loaded node. The reason is that, at the loaded node $c = z$. Consequently, the first term in Equation (6) becomes singular. In this case, Equation (6) can be used after replacing the first term that might yields to zero. In this case, the point load is substituted by an equivalent uniform load, which is then integrated over the replaced loaded area. Assuming a replacement rectangular uniformly loaded area, the required term in Equation (6) can be found by integration as follows($z = c \neq 0$):

$$C_1 = \frac{3-4\nu_s}{2}\left(\frac{1}{a}\ln\frac{(m+a)}{(m-a)}+\frac{1}{b}\ln\frac{(m+b)}{(m-b)}\right) \quad \textbf{(33)}$$

where:

a, b Sides of the loaded rectangular area, [m], and $m = \sqrt{a^2 + b^2}$

Therefore, the settlement $Wr_{i,j}$ [m] at a node i on the raft due to a contact force Qr_j acting at another node j is given by:

$$Wr_{i,j} = Cr_{i,j}\, Qr_j \quad \textbf{(34)}$$

where:

$Cr_{i,j}$ Flexibility coefficient of node i due to a contact force Qr_j on node j, [m/kN],
$Cr_{i,j} = f_{i,j}$ for $i \neq j$
$Cr_{i,j} = C_{i,i}$ for $i = j$ and $z = c = 0$
$Cr_{i,j} = f_{i,j}$ with modified term C_1 for $i = j$ and $z = c \neq 0$

For a raft of n_r nodes, the settlement form can be expressed in matrix as:

$$\{Wr\} = [Cr]\{Qr\} \quad \textbf{(35)}$$

where:

$\{Wr\}$ n_r vector of settlements of raft nodes due to contact forces on the raft,
$[Cr]$ $n_r \times n_r$ matrix of raft flexibility coefficients due to unit contact forces on the raft, and
$\{Qr\}$ n_r vector of contact forces acting on the raft.

The total settlement in the raft due to all forces in the piled-raft system is given by:

$$\{Wt\} = \{Wb\} + \{Ws\} + \{Wr\} \quad \textbf{(36)}$$

Substituting from Equations (31), (32) and (35) into Equation (36), it can be found that:

$$\{Wt\} = [Cb]\{Qb\} + [Cs]\{Qs\} + [Cr]\{Qr\} \quad \textbf{(37)}$$

where:

$\{Wt\}$ n_r vector of total settlements in the raft due to all forces in the piled-raft system.

2.6. Formulation of soil equations

Assume that the vector $\{S\}$ represents the total settlements in the raft mesh due to all forces in the piled-raft system. This vector should have a size of $n=n_p+n_r$ to include the settlements of the raft nodes and the piles all together. The vector of total settlements can be obtained from:

$$\{S\} = \begin{Bmatrix}\{St\}\\ \{Wt\}\end{Bmatrix} \quad \textbf{(38)}$$

Substituting from Equations (28) and (37) into Equation (38), it can be found that:

$$\{S\} = \begin{Bmatrix}[Fb]\{Qb\} + [Is]\{Qs\} + [Cp]\{Qp\} + [Jr]\{Qr\}\\ [Cb]\{Qb\} + [Cs]\{Qs\} + [Cr]\{Qr\}\end{Bmatrix} \quad \textbf{(39)}$$

or

$$\{S\} = \begin{bmatrix}[Cp] & [0]\\ [0] & [Cr]\end{bmatrix}\begin{Bmatrix}\{Qp\}\\ \{Qr\}\end{Bmatrix} + \begin{Bmatrix}[Fb]\{Qb\} + [Is]\{Qs\} + [Jr]\{Qr\}\\ [Cb]\{Qb\} + [Cs]\{Qs\}\end{Bmatrix}$$

Equation (40) can be simplified to:

$$\{S\}=[C]\{Q\}+\{Pr\} \quad \textbf{(41)}$$

where $\{Pr\}$ is given by:

$$\{Pr\}=\begin{Bmatrix}[Fb]\{Qb\}+[Is]\{Qs\}+[Jr]\{Qr\}\\ [Cb]\{Qb\}+[Cs]\{Qs\}\end{Bmatrix} \quad \textbf{(42)}$$

and the term $[C]\{Q\}$ is given by:

$$[C]\{Q\}=\begin{bmatrix}[Cp] & [0]\\ [0] & [Cr]\end{bmatrix}\begin{Bmatrix}\{Qp\}\\ \{Qr\}\end{Bmatrix} \quad \textbf{(43)}$$

where:

$\{Q\}$ n vector of pile loads and contact forces, and

$[C]$ $n\times n$ matrix of flexibility coefficients of the piles and the raft.

From Equation (40) and using matrix inversion, it can be found that:

$$\{Q\}=[Ks]\{S\}-[Ks]\{Pr\} \quad \textbf{(44)}$$

where $[Ks] = [C]^{-1}$ is the soil stiffness matrix of the piles and the raft, which can be given by:

$$[Ks]=\begin{bmatrix}[Kp] & [0]\\ [0] & [Kr]\end{bmatrix} \quad \textbf{(45)}$$

where:

$[Kp] = [Cp]^{-1}$ is a $n_p\times n_p$ diagonal matrix that represents the soil stiffness due to pile self-settlements, and

$[Kr] = [Cr]^{-1}$ is the raft stiffness matrix due to raft-soil interaction.

2.6. Analysis of rigid piled-raft

Figure 5 shows a rigid piled-raft for which the settlement can be defined by the rigid body translation w_o at the center of the raft, in addition to two rotations θ_x and θ_y about the x and y axes, respectively. Realizing that the raft exposes a rigid body movement, the settlement S_i at any node on the raft, with coordinates (x_i, y_i) from the center of area of the raft, is given by:

$$S_i = w_o + x_i \tan\theta_y + y_i \tan\theta_x \quad \textbf{(46)}$$

For the entire piled-raft system, Equation (46) can be rewritten in a matrix form as:

$$\{S\}=[X]^T\{\Delta\} \quad \textbf{(47)}$$

where:

$\{\Delta\}$ 3×1 displacement vector, and

$[X]^T$ $n\times 3$ cartizian coordinates matrix.

For equilibrium the following conditions must be satisfied:

- The resultant of the external vertical forces acting on the raft is equal to the sum of contact forces and pile loads.
- The moment of resultant of the external vertical forces about either x-axis or y-axis is equal to the sum of moments induced by the contact forces and pile loads about either axis.

Assuming that Q_i represents either the pile load Qp or the contact force Qr at any node i on the mesh, then:

$$\left.\begin{aligned} N &= Q_1+Q_2+Q_3+\ldots+Q_n\\ N.e_x &= Q_1.x_1+Q_2.x_2+Q_3.x_3+\ldots+Q_n.x_n\\ N.e_y &= Q_1.y_1+Q_2.y_2+Q_3.y_3+\ldots+Q_n.y_n\end{aligned}\right\} \quad \textbf{(48)}$$

where:

N Resultant of the applied loads acting on the raft, [kN],

$N\,e_x$ Moment due to resultant N about x-axis, $M_x = N\,e_x$, [kN.m],

$N\,e_y$ Moment due to resultant N about y-axis, $M_y = N\,e_y$, [kN.m],

e_x, e_y Eccentricities of the resultant about x- and y-axes, [m], and

x_i, y_i Coordinates of the load Q_i, [m].

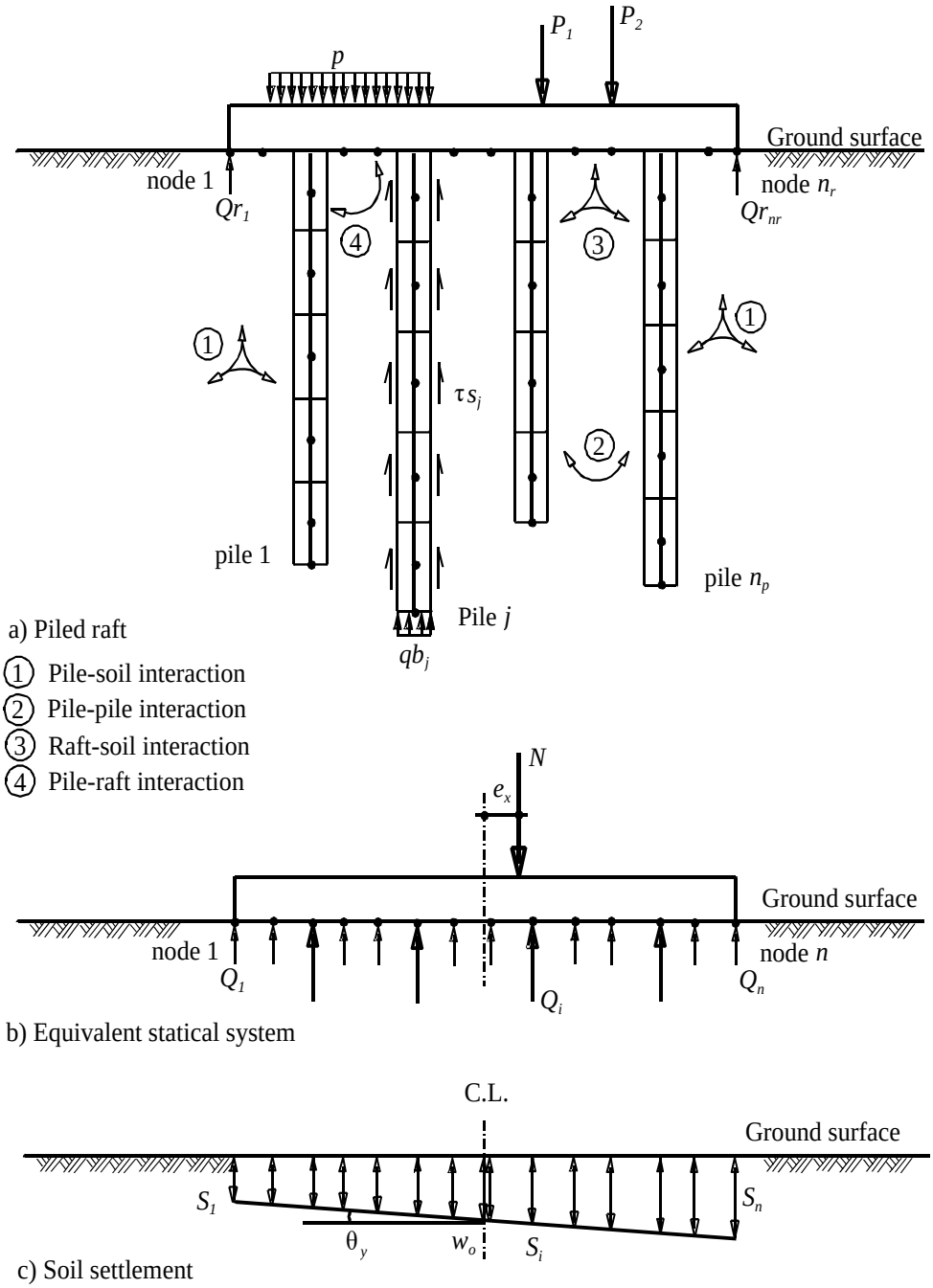

Fig. (5): Modeling of rigid piled-raft

For the entire piled-raft foundation, Equation (48) can be rewritten in a matrix form as:

$$\{N\} = [X]\{Q\} \quad \textbf{(49)}$$

where $\{N\}$ is the vector of resultant force and moments.

Substituting from Equations (44) and (47) into Equation (49), the following linear system of equations is obtained:

$$\{N\} = [X]\left([Ks][X]^T\{\Delta\} - [Ks]\{Pr\}\right) \quad \textbf{(50)}$$

(50)

From Equations (49) and (50), one gets

$$\{Q\} = [Ks][X]^T \{\Delta\} - [Ks]\{Pr\} \quad \textbf{(51)}$$

The system given in Equation (50) should be solved to get the displacements w_o, tan θ_x, and tan θ_y. The displacement values w_o, tan θ_x and tan θ_y are substituted into Equations (47) and (51) to find *n* pile settlements, and the *n* pile loads and contact forces,

2.7. Analysis of a rigid pile group or a flexible raft on a rigid pile group

Analysis of a rigid pile group is easier; if compared to either a flexible or a rigid piled-raft. In this case, the contact forces {*Qr*} and settlements at raft nodes {*Wt*} are omitted from above formulation. Therefore, Equations (42) and (43) can be simply rewritten as:

$$\{Pr\} = \{[Fb]\{Qb\} + [Is]\{Qs\}\} \quad \textbf{(52)}$$

$$[C]\{Q\} = [Cp]\{Qp\} \quad \textbf{(53)}$$

For a flexible pile raft, in which the group of piles is subjected to a known system of loads {*Qp*} and {*Qr*}, Equation (40) may be used directly to evaluate the settlement of each pile in the group.

2.7. Iteration method

The developed linear equation system is solved iteratively by computing the pile stiffness due to its self-settlement. This may be achieved by using either the modified or any empirical load-settlement relationship. This pile stiffness is simply added to the raft stiffness. Then, the piled-raft is solved iteratively until the compatibility among the settlements of raft, piles and soil is fulfilled. The above mentioned formulation was implemented into the software *ELPLA* (Kany, M. *et al.*, 2007), in order to perform the analysis of piled raft using the considered international codes. As shown in Figure 6, the iterative process is carried out as follow:

1. Generate the flexibility matrices due to pile-pile, pile-raft and raft-soil interactions, [*Fb*], [*Is*], [*Cb*], [*Cs*], [*Jr*] and [*Cr*].
2. Find the soil stiffness matrix of the raft due to raft-soil interaction, [Kr] = [Cr]-1.
3. Using loads acting on the raft, assume an average stress for raft nodes and piles, then find the initial loads for the piles {Qp} and the initial forces for other raft nodes {Qr}.

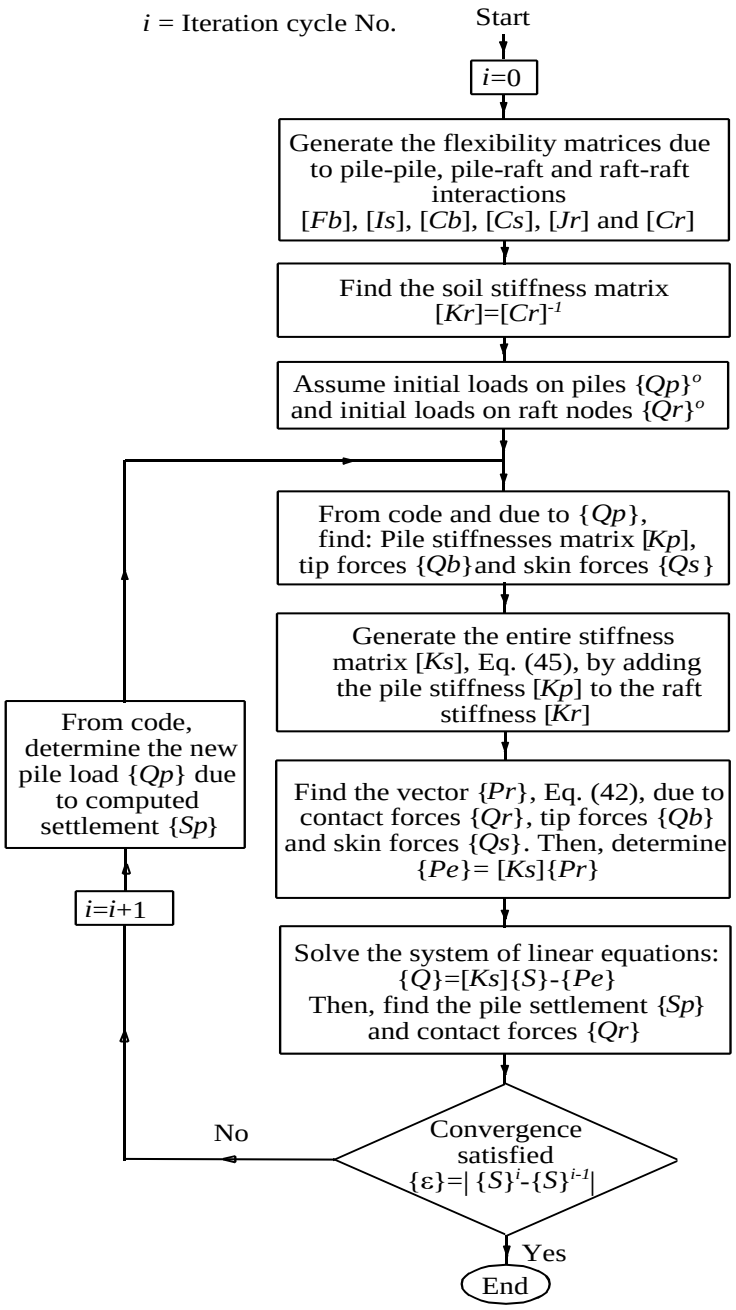

Fig. (6): Flowchart of the iterative procedure.

4. From the modified or the empirical load-settlement curves, find the coefficients of pile stiffness matrix [*Kp*].
5. Generate the entire stiffness matrix [K*s*] for the pile-raft system by adding the pile stiffness matrix [K*p*] to the raft stiffness [K*r*].
6. Determine the vector {*Pr*} in Equation (42) due to the contact forces and the total force acting on each pile.
7. Perform the analysis of piled-raft system to get the pile settlements {*Sp*} and contact forces {*Qr*}.
8. Compare the settlement from cycle *i* with that of cycle *i*+1 to find the accuracy of the solution.
9. If the accuracy from step 8 is less than a specified tolerance ε, determine the new pile loads {*Qp*} corresponding to the computed settlements {*Sp*}. This may be achieved by using either the modified or the empirical load-settlement curves.

Steps 4 to 9 are repeated until reaching an acceptable accuracy, which ensures the compatibility among the settlements of piles, raft and soil at all interfaces.

3. Numerical results and validation

To confirm the validity and efficiency of the proposed analysis, nine case histories of piled-raft systems around the world, are re-analyzed herein. The buildings are 43 [m] to 256 [m] in height above the ground surface and were completed in 1983-2009. For all cases, field measurements have been performed to monitor the foundation settlements and the load sharing among the rafts and the piles. Figure 7 shows a general description of each of the nine case histories under consideration. Besides the wide range of building heights, a wide variety of raft geometric shapes and pile distributions, are covered as shown in the figure. Table 1 presents the main characteristics and field measurements of each case.

The pile self-settlement in the present mixed analysis of piled raft is modeled empirically using any of the following international codes: ECP202, 2005; DIN4014, 1990; AASHTO, 2005; and French Code, 1993. Besides, the hyperbolic modified load-settlement curves (El-Gendy *et al.*, 2013) are also investigated. Regarding the four mentioned codes, the authors previously showed that the load-settlement relationship of AASHTO is the least conservative, while that of the Egyptian and French codes were relatively conservative, (El-Gendy *et al.*, 2013).

To facilitate the presentation of results, the following labels are used in the following sections to distinguish the results for different methods:

MLSC1	=	modified load-settlement curve for a single pile based on AASHTO,
MLSC2	=	modified load-settlement curve for a single pile based on ECP 202,
NPRE	=	analysis using pile self-settlement curve of the Egyptian code ECP 202,
NPRD	=	analysis using pile self-settlement curve of the German code DIN 4014,
NPRA	=	analysis using pile self-settlement curve of AASHTO,
NPRF	=	analysis using pile self-settlement curve of the French Code,
NPRM1	=	analysis using the modified hyperbolic pile load-settlement curves, following the ultimate loads and settlements of AASHTO, and
NPRM2	=	analysis using the modified hyperbolic pile load-settlement curves, following the ultimate loads and settlements of ECP 202.

It should be noticed that the three fixed starting letters in each of the above abbreviations refer to the **N**onlinear analysis of **P**iled-**R**aft. Detailed numerical results are given hereafter for the following three case histories:

a) Messeturm building (Frankfurt),
b) Westend one tower, and
c) Forty-seven-story residential tower (Japan).

For each of the three-case histories, the general description of the building is given, followed by the properties of the foundation and underlain soil. Then, the empirical- and proposed load-settlement curves for the different piles used in each case, are shown. Finally, the numerical results are presented and discussed. For the other 6-case histories, final results are summarized and compared to the measured values in separate tables, due to space limitation.

3.1 Piled-raft foundation of Messeturm building.

Messeturm was the tallest high-rise building in Europe until 1997. The building lies in Frankfurt city in Germany. It is 256 [m] in high and standing on a piled-raft foundation. Using instruments installed inside this foundation, an extensive measuring program was established to monitor the behavior of the building. These instruments record raft settlements, raft contact pressures, and loads on pile heads and along the pile shafts. The behavior of Messeturm had been studied by many authors, such as (Sommer & Katzenbach, 1990; Katzenbach *et*

al., 2000; Reul & R&olph, 2003; Chow & Small 2005; Sales *et al.*, 2010; Eslami *et al.*, 2011). Figure 8 shows the Messeturm piled-raft as given by Chow & Small 2005. The building has a basement with two underground floors and 60 stories with a total estimated load of 1880 [MN]. The foundation is a square piled-raft of 58.8 [m] side founded on Frankfurt clay at a depth 14 [m] below the ground surface. Raft thickness varies from 6 [m] at the middle to 3 [m] at the edges. A total of 64 bored piles with equal diameters of 1.3 [m] are arranged under the raft in 3 rings. Pile lengths vary from 26.9 [m] for the 28 piles in the outer ring, to 30.9 [m] for the 20 piles in the middle ring, and to 34.9 [m] for the 16 piles in the inner ring. The underlain soil consists of gravel and sand down to 8 [m] below the ground surface, followed by layers of Frankfurt clay extending to a great depth of more than 100 [m] below the ground surface. The groundwater level lies at 4.75 [m] under the ground surface. The construction of Messeturm started in 1988 and finished in 1991. The recorded settlement at the center of the raft in March 1990 was 8.5 [cm] (Katzenbach *et al.*, 2000), while the recorded settlement in 2001 was 14.4 [cm], (Sales *et al.*, 2010, and Eslami *et al.*, 2011). The expected final settlement, in this case, would be between 15 [cm] and 20 [cm], (Sommer & Katzenbach, 1990).

3.1.1 Soil properties for Messeturm building (Frankfurt)

According to (Reul & Randolph, 2003), Young's modulus of the sand with gravel layer under the raft is E = 75000 [kN/m^2]. Young's modulus for reloading is taken as W = 3 E. Based on a back analysis after (Amann *et al.*, 1975), the distribution of the modulus of compressibility for loading of Frankfurt clay with depth is defined by the following empirical formula:

$$E_s = E_{so}\left(1 + 0.35\, z\right) \qquad \textbf{(54)}$$

While that for reloading is:

$$W_s = 70\left[\mathrm{MN/\,m^2}\right] \qquad \textbf{(55)}$$

where:

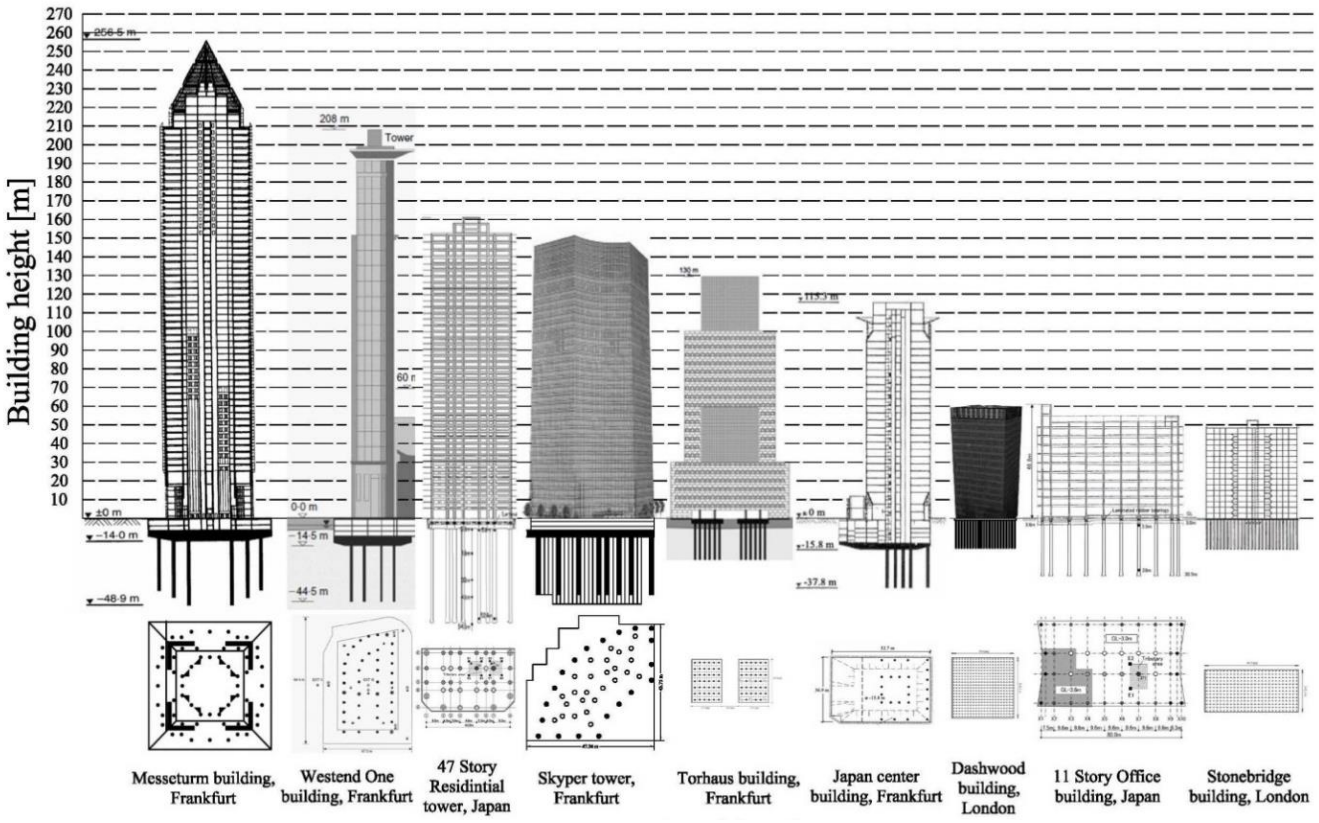

Fig. (7): Geometrical descriptions of piled-raft case histories under consideration

Table 1 Main characteristics and field measurements of considered case histories

No.	Case study	Site location	P	H [m]	T [MN]	Piled-raft description							Measured values		Reference
						Foundation				Piles					
						L [m]	W [m]	Th [m]	D [m]	N	Di [m]	L [m]	S [cm]	B [%]	
1	Messeturm	Frankfurt	1988:1991	257	1880	59	59	3.00-6.00	14	64	1.3	26.9-34.9	14.4	40	(Sales *et al.*, 2010)
2	Westend Tower	Frankfurt	1990:1993	208	895	62	47	4.65	15	40	1.3	30	12	50	(Reul & Randolph ,2003)
3	forty-seven-story residential tower	Japan	2005:2009	162	969	45	29	2	4.3	6 10 16 4	1.9 1.8 1.6 1.5	50	2.9	82	(Yamashita *et al.*, 2011)
4	Skyper	Frankfurt	2002:2004	154	818	47	47	3.5	12	46	1.5	6.27	3.1	-	(Sales *et al.*, 2010)
5	Torhaus	Frankfurt	1983:1986	130	400	25	18	2.5	3	42	0.9	20	12	64	(Eslami *et al.*, 2011)
6	Taunustor Japan Centre office	Frankfurt	1994:1996	115	1050	53	37	1.0-3.0	16	25	1.3	22	5	-	(Katzenbach *et al.*, 2000)
7	Dashwood	London	1973:1976	61	274	43	32	0.9	1	462	0.5	15	3.1	93-100	(Hong *et al.* 1999)
8	Eleven story building	Japan	2004:2005	61	692	80	44	0.8	3	40	1.4	27.5	1	54	(Yamashita *et al.*, 2011)
9	Stonebridge Tower.	London	1973:1975	43	156	43	19	0.9		351	0.5	13	1.8	93-100	(Hemsley, 2000)

P (Construction period), H (Maximum height), T (Total load), L (Length), W (Width), Th (Raft thickness), D (Depth), N (Number), Di (Diameter), S (Settlement), B (Bearing factor)

E_s Modulus of compressibility for loading, [MN/m^2],
E_{so} Initial modulus of compressibility, E_{so}=7 [MN/m^2],
Z Depth measured from the clay surface, [m], and
W_s Modulus of compressibility for reloading, [MN/m^2].

According to (Sommer & Katzenbach, 1990), the undrained cohesion c_u of Frankfurt clay increases with depth from c_u=100 [kN/m^2] to c_u=400 [kN/m^2] in 70 [m] depth under the clay surface. Poisson's ratio of the soil is taken as ν_s = 0.25 [-].

3.1.2 Raft and pile material

The raft has the following material parameters:
Young's modulus E_b = 3.4 x 107 [kN/m^2],
Poisson's ratio ν_b = 0.2 [-], and
Unit weight γ_b = 25 [kN/m^3].

While piles have the following material parameters:
Young's modulus E_b = 2.35 x 107 [kN/m^2], and
Unit weight γ_b = 25 [kN/m^3].

3.1.3 Analysis of the piled-raft

Measured settlements and pile load ratios given by (Sales *et al.*, 2010), are compared to those predicted by the proposed numerical methods. By realizing that the piled-raft system under consideration is completely symmetric, the numerical model was built for one-quarter only of the piled-raft. The raft is divided into elements with a maximum side length of 2.5 [m] as shown in Figure 9. Similarly, the piles are divided into elements of 2.0 [m] length; as a maximum.

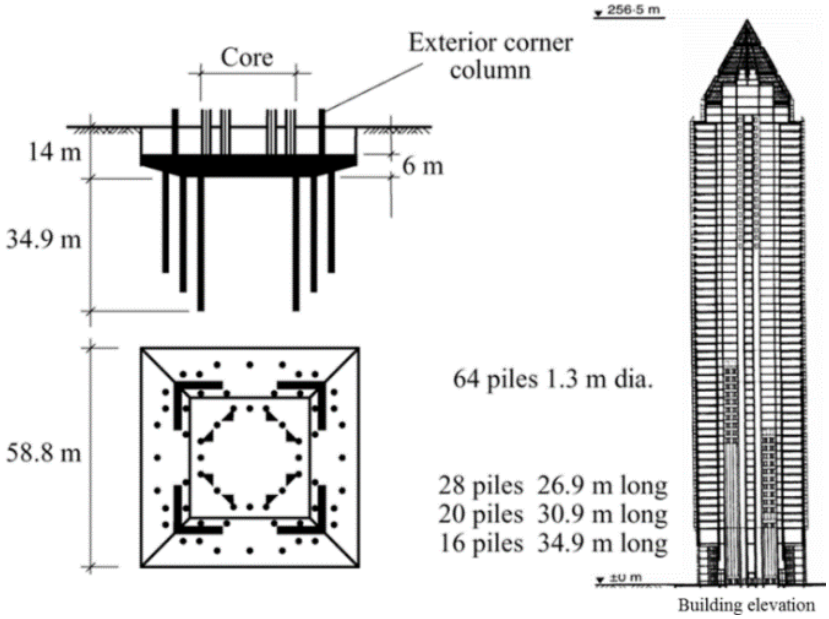

Fig. (8): Messeturm piled-raft details, after (Chow & Small, 2005)

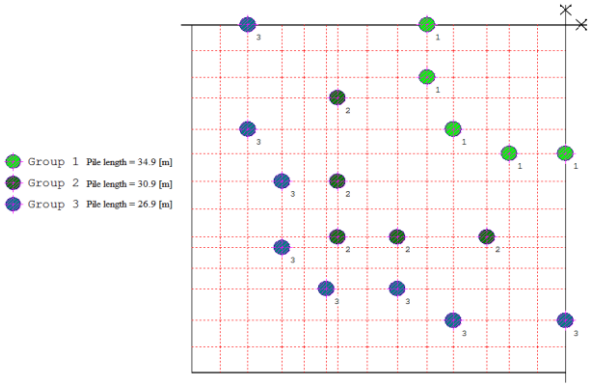

Fig. (9): FE Mesh of Messeturm piled-raft

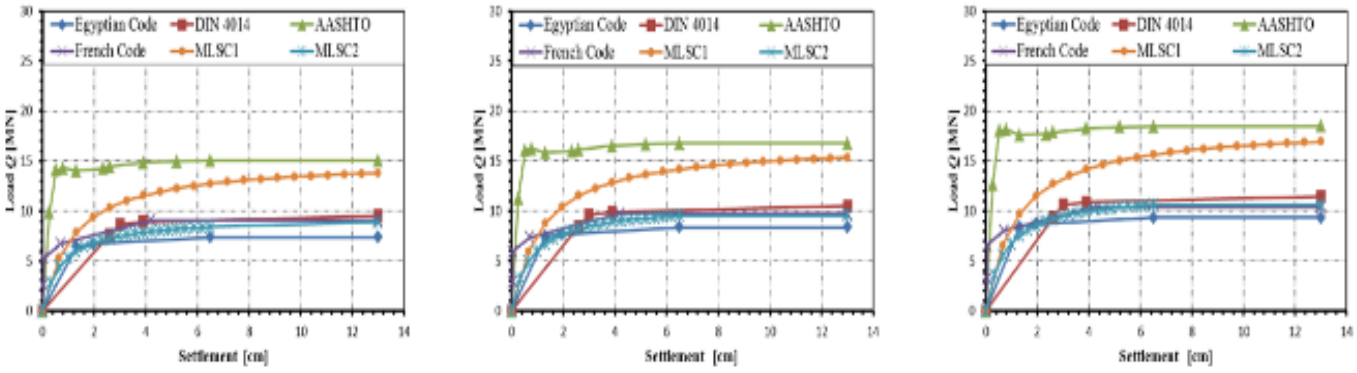

(a) Pile length = 26.9 [m]. (b) Pile length = 30.9 [m]. (c) Pile length = 34.9 [m].

Fig. (10): Single pile load-settlement curves for Messeturm building.

Table 2 Comparison between predicted and measured results

Type of analysis	Settlement		Bearing factor	
	[cm]	[%]	[%]	[%%]
Measured	14.40	-	40	-
NPRE	17.29	+20	32	-20
NPRD	15.37	+7	40	0
NPRA	10.83	-25	59	+48
NPRF	15.92	+11	38	-5
NPRM1	12.07	-16	54	+35
NPRM2	16.01	+11	37	-7

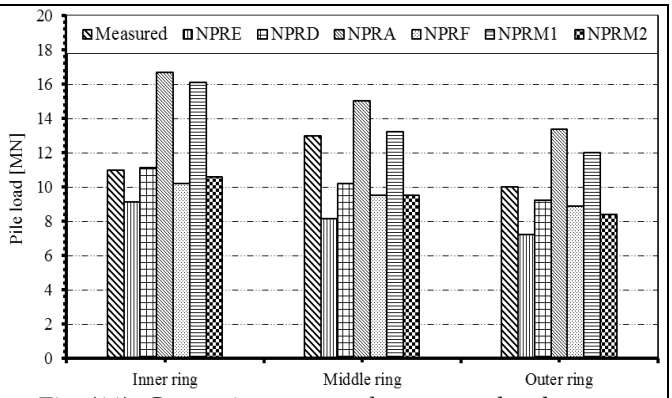

Fig. (11): Comparison among the measured and predicted pile loads

3.1.4 Comparison between numerical predictions and field measurements

For each of the three types of piles used in Messeturm building, Figure 10 shows a comparison among the load-settlement curves given by each of the four considered codes under consideration, in addition to the proposed hyperbolic models. Effect of variation of pile length among the three types of piles is evident as shown in the figure. The numerical results of central settlement and bearing factor of piled-raft are listed in **Error! Reference source not found.**Table 2. The results are given for the four codes and the couple of modified load-settlement curves (NPRE, NPRD, NPRA, NPRF, NPRM1, and NPRM2). Moreover, Figure 11 shows a comparison among the measured and predicted pile loads at different locations in the building. As clear from Table 2, the percentage difference of the predicted central settlement using the rigid method, is (-25% to +20%) of the measured settlement. The percentage difference of the predicted pile load-bearing ratio is (-20% to +48%) of the measured value. Table 2 reveals also that the predictions showed an acceptable match with the measured values many times.

3.2 Piled-raft of Westend One Tower

Many authors had studied Westend tower behavior such as (Reul & Randolph, 2003; and Poulos, 2011). Westend one tower was constructed between 1990 and 1993 in Frankfurt, Germany. The 208 m-high tower and the 60 m-high low-rise section of the building complex are founded on two separated rafts. The piled-raft of the tower consists of a 47 [m] by 62 [m] large raft with a thickness of 3.00 to 4.65 m and 40 bored-piles with a length of 30 [m] and 1.3 [m] in diameter. The bottom of the raft lies 14.5 m below ground level as shown in Figure 12-a. The groundwater level is situated at 7 [m] below ground level. The layout of the measurement devices is shown in Figure 12-b. The low-rise section of the building complex is not considered in the analysis. The maximum load above the raft is about 895 MN applied in the core area of the raft.

3.2.1 Properties of materials

The bottom of the Frankfurt clay is assumed to be 68 [m] below the foundation level, which is existing at 14.5 [m] below the ground level. The Frankfurt clay is followed by a 32 [m] thick layer of Frankfurt limestone. Poisson's ratio of the clay is taken as $\nu s = 0.15$ [-]. The distribution of Young's modulus of the clay with depth is described by the following empirical formulation based on the back-analysis of boundary value problems in Frankfurt clay, (Reul, 2000):

$$E = 45 + 0.7\,z\left[\tanh\left(\frac{z-30}{15}\right)+1\right] \tag{56}$$

where E is Young's modulus of the clay [MPa], and z is the depth from the clay layer surface [m]. All raft and pile material parameters are the same as those given above for the Messeturm building. However, for the reinforced concrete of piles, *Young's* modulus E_b is 2.2 x 10^7 [kN/m^2] based on the investigations performed by (Franke & Lutz,1994).

3.2.2 Comparison between numerical predictions and field measurements

The finite element mesh of the piled-raft is shown in Figure 13. The settlement measured at the foundation center reached 12.0 [cm] after thirty months after the completion of the shell of the building. The corresponding measured pile bearing factor was found to be about 50 [%], under the assumption that the average load of the six instrumented piles is equal to the average load of the whole pile group. Measured results for settlement and pile bearing ratio, are compared herein to the numerical predictions of the present analyses obtained using the rigid method. Figure 14 depicts the load-settlement relationships for a single pile based on the pile parameters and soil properties given above. The numerical results of the present mixed numerical method are listed in Table 3. For this case history, the percentage difference of the predicted settlement is (-17% to +6%) of the measured settlement. The percentage difference of the predicted pile load-bearing ratio is (-48% to -14%) of the measured value. The predicted

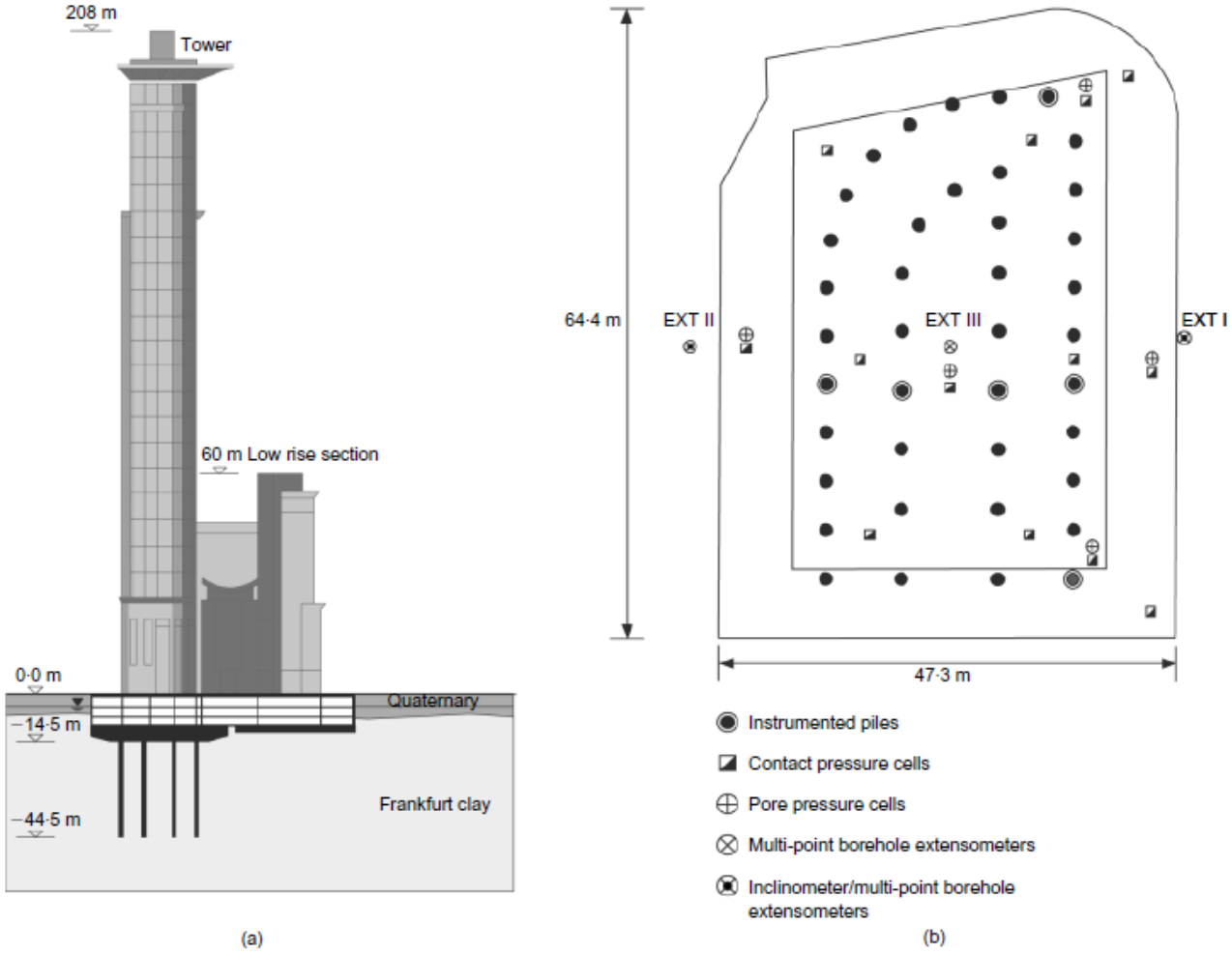

settlements for different methods are mostly satisfactory; however, the predictions of pile-load ratios are relatively underestimated.

Fig. (12): Layout of Westend one tower. (a) Elevation. (b) Piled-raft plan, after (Reul & Randolph, 2003)

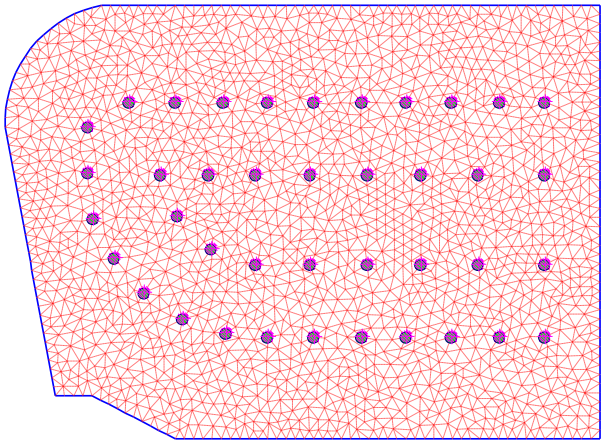

Fig. (13): FE mesh of the piled-raft for Japan residential building

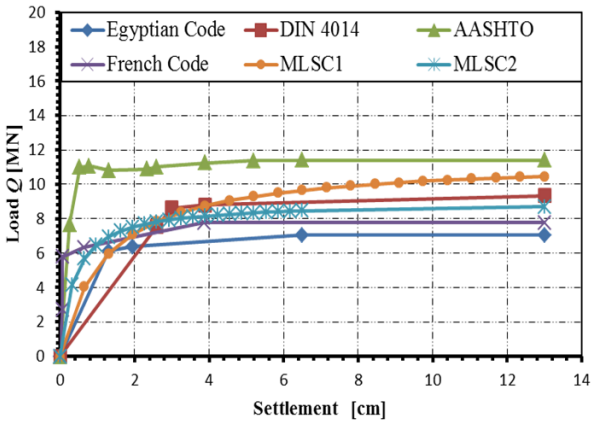

Fig. (14): Westend one tower single pile load-settlement curves

3.3 Piled-raft of forty-seven story residential tower (Japan)

The third case history listed in Table 1 comprises a reinforced concrete 47-story residential tower lies in Nagoya, Aichi Prefecture in Japan. It is 162 [m] high above the ground surface and the foundation measuring 50 [m] by 34 [m] in plan. The building foundation was instrumented to measure the displacements below the raft using differential settlement gauges as stated by (Yamashita *et al.*, 2011). The average contact pressure over the raft was 600 [kPa]. The raft is located 4.3 [m] below the ground surface and founded on medium-to-dense sand and gravel. A piled-raft system consisting of 2 [m] thick raft and 36 cast-in-place concrete piles was executed; to reduce the differential settlement. The pile length is 50 [m], and the diameter varies from 1.5 to 1.9 [m] in four different groups as shown in Figure 15.

3.3.1 Properties of materials

According to (Yamashita *et al.*, 2011), the soil profile down to a depth of 4 [m] from the ground surface consists of fill and silt. Below this layer lies medium to dense sand, and gravel down to a depth of 17 [m] with an SPT range from 20 to 30, underlain by medium silt. Between depths of 27 to 43 [m], there lies dense sand, very dense sand and gravel, and medium to dense sand with an SPT range from 20 to 60 or higher. Below the depth of 43 [m] there lies very dense sand and gravel. The groundwater table appears about 2.5 [m] below the ground surface. *Poisson's* ratio of the soil was taken as $\nu s = 0.30$ [-]. Figure 16 summarizes the soil layers and their properties. All raft and pile material parameters were taken the same as those given above for Messeturm building.

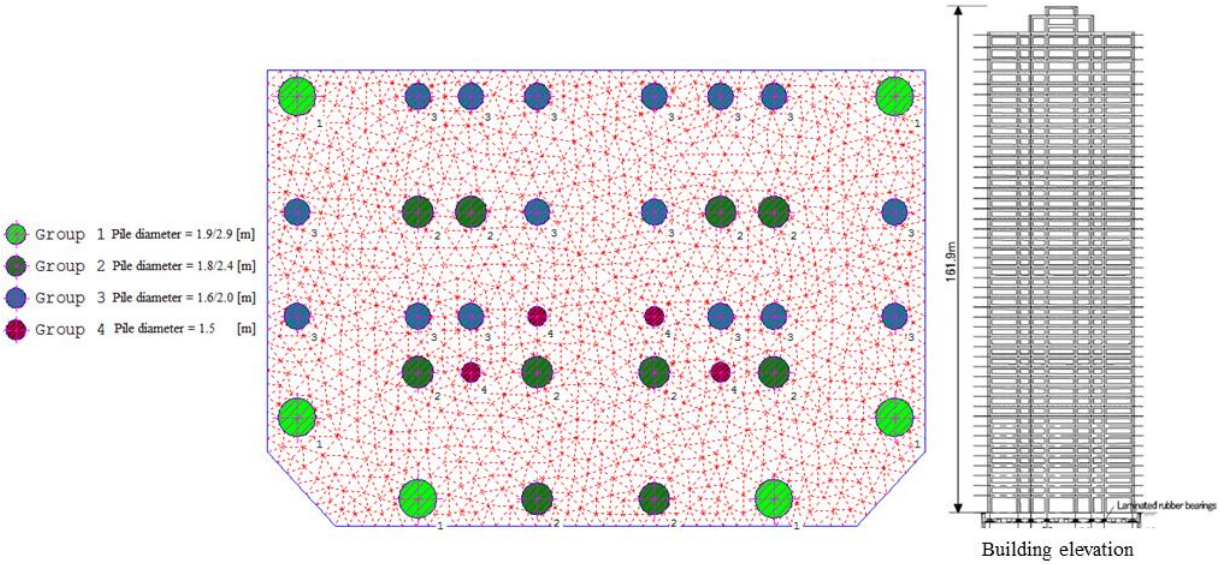

Fig. (15): FE mesh of the piled-raft for forty-seven story residential tower (Japan)

3.3.2 Comparison between numerical predictions and field measurements

According to (Yamashita *et al.*, 2011), the maximum settlement measured at the raft center reached 2.90 [cm], while the piles bearing factor was found to be 82 [%] after 17 months of the building completion. The load-settlement relationships for two of the four pile types used in the construction are shown in Figure 17. The effect of the variation of pile and base diameters on the pile ultimate load is evident. Comparisons of the measured and theoretically predicted results using the rigid method for the settlement and pile-bearing ratio are given in Table 4. The predicted settlement at the raft center for the different methods varies from 3.46 to 4.44 [cm], versus 2.9 [cm] measured settlement. Predictions of the pile load-bearing ratio for all methods are very close to each other (about 73% of the measured ratio).

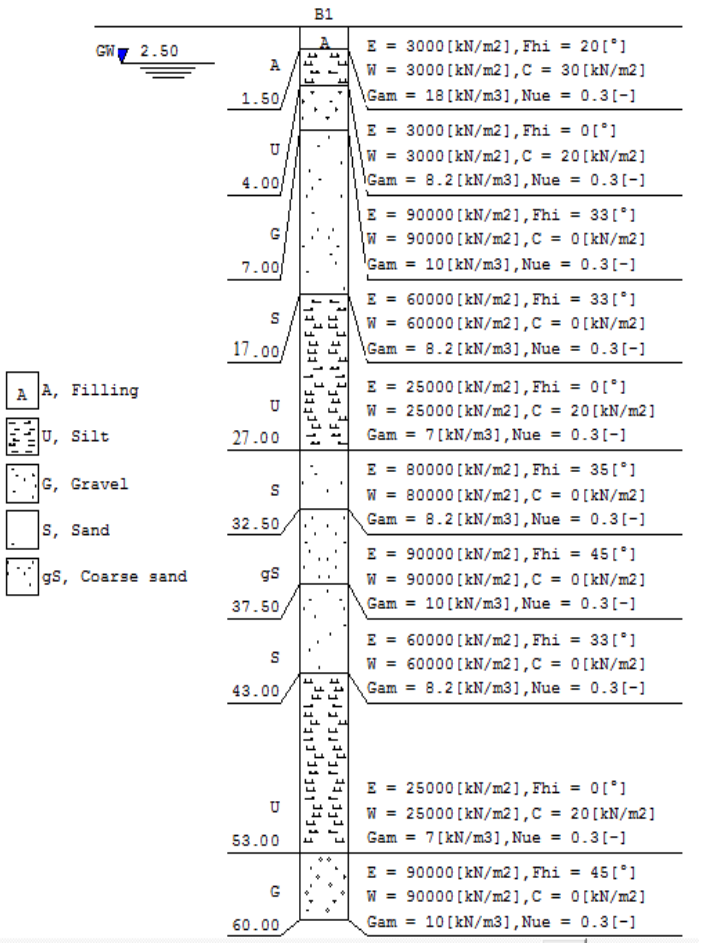

Fig. (16): Boring logs

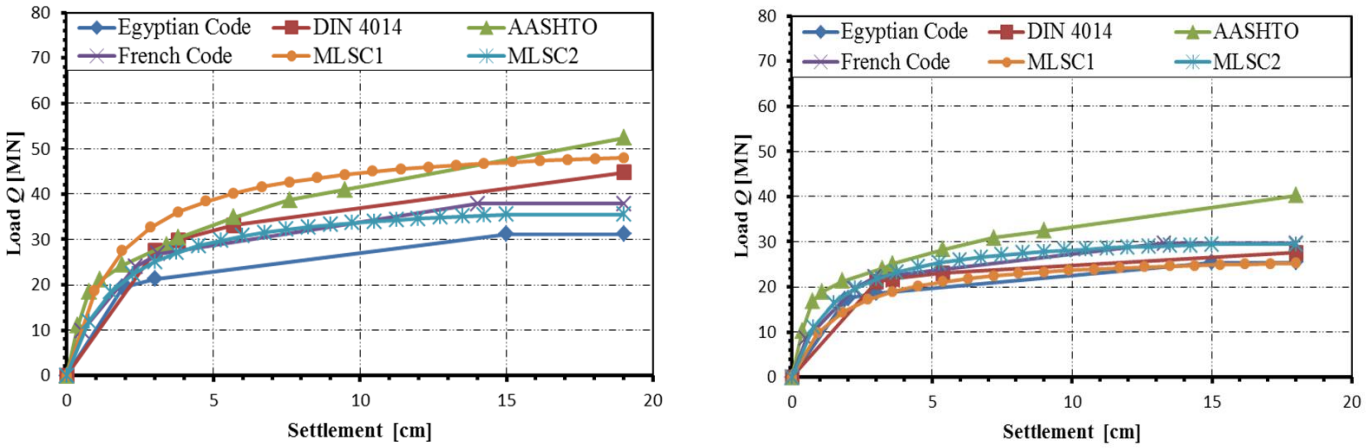

(a) Diameter = 190 [cm]. **(b) Diameter = 180 [cm].**

Fig. (17): Japan residential building single pile load-settlement curves

Table 4 Comparison between predicted and measured results

Type of analysis	Settlement		Bearing factor	
	[cm]	[%]	[%]	[%%]
Measured	2.90	-	82	-
NPRE	4.44	53	58	-29
NPRD	3.63	25	61	-26
NPRA	3.66	26	61	-26
NPRF	3.98	37	60	-27
NPRM1	3.46	19	62	-24
NPRM2	4.13	42	59	-28

3.4 Comparison of summarized results for all case histories

The main characteristics and field measurements of all considered case histories are listed in Table 1. Due to space limitation, it could not be possible to present more details about the last six case histories. For more details about those case histories, the reader may refer to the references indicated in Table 1. Comparisons between the predictions and the available measurements for each of the nine case histories, are listed in Tables 5 and 6. Besides the measured and predicted results, the two tables give the ratios of predicted to measured settlement, and pile load sharing (P/M). Both the best and worst predictions are given in each case. A careful study of the results given in Tables 5 and 6 shows that:

a) All codes under consideration (ECP202, 2005; DIN4014, 1990; AASHTO, 2005; and French Code, 1993), as well as the proposed modified load-settlement models could successfully complete the analysis of piled-raft following the presented formulation. Moreover, the present analysis could satisfactorily predict both the raft settlement and the pile load-sharing; for most cases.

b) Although, the predicted results are sensitive to the adopted load-settlement model of a single pile, yet they are still acceptable for most models.

c) Predicted settlements of the present analysis (NPRA) using the AASHTO code are mostly the farthest from the measurements, if compared to the predictions of other models. However, they are still adequately accurate for case histories 4 and 9.

d) For most case histories, predictions of NPRM1 analysis are closer to the measurements, if compared to NPRA analysis. The same is true with respect to the NPRM2 analysis; which improves the predictions of the NPRE analysis in most cases.

For case histories 7 and 9, it can be seen from Table 6 that the pile load-sharing reaches 100%, for both measured and predicted results. For those cases, the foundation system works as a free-standing pile group and piles could attract the applied loads completely (with no raft-soil interaction). For both case histories, the pile spacing in both directions is about three times as large as the pile diameter.

4. Conclusions

Modeling the self-settlement of a bored pile as given by the Egyptian, German, American, and French codes (ECP202, 2005; DIN4014, 1990; AASHTO, 2005; French Code, 1993), in the context of a mixed nonlinear analysis of a piled-raft system, is validated. Moreover, using the hyperbolic load-settlement model proposed previously by the authors (El-Gendy *et al.*, 2013), instead of the empirical code relationships is also validated. In the proposed numerical approach, the finite layer method is used for analyzing the layered soil, whereas the piles and the raft are analyzed using the finite element method. Settlements due to pile-pile, pile-raft, and raft-soil interactions are determined using flexibility coefficients according to the elasticity theory. The analysis is carried out iteratively,

Table 5 Summary of settlement results at raft center for all case histories

Case history		Measured settlement [cm]	Predicted settlement [cm]						P / M ratio	
			NPRE	NPRD	NPRA	NPRF	NPRM1	NPRM2	best	worst
1	Messeturm	14.40	17.29	15.37	10.83	15.92	12.07	16.01	1.07	0.75
2	Westend 1	12.00	12.71	11.38	9.96	12.13	11.22	12.07	1.01	0.83
3	47 story res. tower	2.90	4.44	3.63	3.66	3.98	3.46	4.13	1.19	1.53
4	Skyper tower	3.10	3.52	3.09	2.86	3.33	3.35	3.35	0.99	1.14
5	Torhaus	12.40	11.52	11.84	7.69	9.11	8.52	10.11	0.95	0.62
6	Japan center	5.00	4.56	4.33	3.34	4.24	3.89	4.34	0.91	0.67
7	Dashwood house	3.30	2.84	2.95	2.44	2.75	2.74	2.76	0.89	0.74
8	Eleven story building	1.00	1.41	1.31	1.43	1.43	1.37	1.40	1.31	1.43
9	Stonebridge Tower.	1.80	1.66	2.10	1.72	1.92	1.87	1.93	1.04	1.17

Table 6 Summary of pile load ratio results at raft center for all case histories

Case history		Measured bearing factor [%]	Predicted bearing factor [%]						P / M ratio	
			NPRE	NPRD	NPRA	NPRF	NPRM1	NPRM2	best	worst
1	Messeturm	40%	32%	40%	59%	38%	54%	37%	1. 00	0.82
2	Westend 1	50%	26%	34%	43%	30%	35%	30%	0.86	0.52
3	47 story res. tower	82%	58%	61%	61%	60%	62%	59%	0.76	0.71
4	Skyper tower	-	44%	50%	52%	46%	46%	46%	-	-
5	Torhaus	64%	49%	65%	69%	62%	66%	56%	1.02	0.77
6	Japan center	-	17%	20%	32%	21%	25%	20%	-	-
7	Dashwood house	100%	100%	100%	100%	100%	100%	100%	1.00	1.00
8	Eleven story building	54%	33%	37%	33%	33%	35%	34%	0.69	0.61
9	Stonebridge Tower.	100%	100%	100%	100%	100%	100%	100%	1.00	1.00

and the compatibility of settlements at the raft, piles, and soil interfaces are fulfilled for each computational cycle. Comparisons with the published field measurements for nine-case histories proved the efficiency and validity of the present numerical method. Based on the analyses performed in this research, the following conclusions could be drawn:

a) Analysis of piled-raft systems comprising large-diameter bored piles could successfully be completed by modeling the pile self-settlement using any of the four codes under consideration (ECP202, 2005; DIN4014, 1990; AASHTO, 2005; French Code, 1993), or by using the hyperbolic load-settlement model, (El-Gendy *et al.*, 2013).

b) Owing to its simple form, the hyperbolic load-settlement model (El-Gendy *et al.*, 2013) could mostly facilitate the iterative computations of piled-raft analysis.

c) Based on the numerical predictions obtained for the investigated nine-case histories, DIN 4014 was mostly the code that gave the closest match to field measurements, while the AASHTO predictions were the farthest. Nevertheless, the AASHTO results may be improved by using the modified load-settlement model MLSC1, (El-Gendy *et al.*, 2013). Predictions of both the Egyptian and French codes (ECP202, 2005, and French Code, 1993), were generally conservative, but they were still acceptable for most case studies.

References

AASHTO: "LRFD bridge designs Specifications", SI units. 3rd Ed. Washington, D.C, (2005)

Amann, P., Breth, H. and Stroh, D.: "Verformungsverhalten des Baugrundes beim Baugrubenaushub und anschließendem Hochhausbau am Beispiel des Frankfurter Ton Mitteilungen", der Versuchsanstalt für Bodenmechanik und Grundbau der Technischen Hochschule Darmstadt, Heft 15, (1975).

Chow, H., and Small, J.: "Behaviour of Piled Rafts with Piles of Different Lengths and Diameters under Vertical Loading", GSP 132 Advanced in Deep Foundations, ASCE, (2005)

DIN 4014, Deutsches institute fur Normung: "German Association for earth works and foundation engineering", (1990).

ECP 202: "Egyptian Code for Soil Mechanics-Design and Construction of Foundations", Part 4, Deep Foundations, (2005)

El Gendy, M., Hanish, J., and Kany, M.: "Empirical nonlinear analysis of piled-raft", Bautechnik 83 Heft 9 pages 604–617, Ernst and Sohn, Berlin, (2006)

El-Gendy, M. M., El-Arabi, I. A., and Kamal, M. A.: "Comparative Examinations of Single Bored Piles Using International Codes", (2013).

Eslami, A., Salehi, S., and Malekshah: "Analysis of non-connected piled-raft foundations (NCPRF) with cushion by finite element method", Comp. Meth. Civil Eng., Vol. 2, 2, 153-168, Copyright by the University of Guilan, November (2011).

Eslami, A., Veiskarami, M. and Eslami, M. M.: "Study on optimized piled-raft foundations (PRF) performance with connected and non-connected piles- three case histories", International Journal of Civil Engineering, Vol. 10, No. 2, June (2012).

Franke, E. and Lutz, B: "Pfahl-Platten-Gru¨ndungs-Messungen", Report for the German Research Council (DFG) No. Fr60-1/11, (1994).

Hemsley, J.: "Design application of raft foundations", Thomas Telford, London; Section 18, (2000).

Hong, D., Chow, Y., and Yong, K.: "A method for analysis of large vertically loaded pile groups", Int. J. Numer. Anal. Meth. Geomech, 23, 243-262, (1999).

Huang, M., Jiu, Y., Jiang, J., and Li, B.: "Nonlinear analysis of flexible piled raft foundations subjected to vertical loads in layered soils", Soils and Foundations, Vol. 57, No.4, 632-644, (2017).

Kany, M., El Gendy, M., and El Gendy, A.: "Analysis and design of foundations by the Program ELPLA", GEOTEC Software, Zirndorf, (2007).

Katzenbach, R., Arslan, U., and Moormann, C.: "Piled raft foundation projects in Germany", Design Applications of Raft Foundations, Hemsley, J.A.; Thomas Telford, London, pp 323-391, (2000).

Mandolini, A., and Viggiani, C.: "Settlement of piled foundations", Géotechnique, 47, No. 4, 791-816, (1997).

MELT-Ministère de l'Equipement, du logement et des transports. Règles Techniques de Conception et de Calcul des Fondations des Ouvrages de Génie Civil (in English: "Technical Rules for the Design of Foundations of Civil Engineering Structures", FASCICULE N°62 -Titre V, Textes Officiels N° 93-3 T.O., 182 pages, (1993)

Mindlin, R.: "Force at a point in the interior of a semi-infinite-solid Physics", 7, S. 195-202, (1936).

Nguyen, N.V., Vinh, L.B., and Vo, T.: "Load-sharing mechanism of piled-raft foundation: a numerical study", European J. of Env. and Civil Eng., (2021). DOI: 10.1080/19648189.2021.2013949

Poulos, Harry, G.: "The de Mello Foundation Engineering Legacy, Soils and Rocks", São Paulo, 34(1): 3-31, Coffey Geotechnics, Sydney, Australia, (2011).

Reul, O. and Randolph, M.F.: "Piled rafts in over-consolidated clay: Comparison of in situ measurements and numerical analysis", Geotechnique, Vol. 53, 3, 301-315, (2003).

Reul, O.: "In-situ measurements and numerical studies on the bearing behavior of piled rafts", PhD thesis, Darmstadt University of Technology, Germany, (2000).

Russo, G.: "Numerical analysis of piled-raft", Int. J. Numer. Anal. Meth. Geomech., 22, 477-493, (1998).

Sales, M. M., Small, J. C. and Poulos, H. G.: "Compensated piled rafts in clayey soils", Can. Geotech. J. Vol. 47: 327-345, (2010).

Sommer, H., and Katzenbach, R.: "Last-Verformungsverhalten des Messeturmes Frankfurt", Main Vorträge der Baugrundtagung in Karlsruhe, Seite 371-380, (1990).

Viggiani, C.: "Pile groups and pile raft behavior", Proc. of the 3rd unit. Geot. Sem. On Deep Foundations on Bored and Auger Piles Ghent, Belgien 19-21- Oct. (1998).

Yamashita, K., Yamada, T., and Hamada, J.: "Investigation of settlement and load sharing on piles rafts by monitoring full-scale structures", Soil and foundations Japanese Geotechnical society, Vol. 51, No.3, 513-532, June (2011).